J. Phase Equilib. Diffus. (2024) 45:417–432
https://doi.org/10.1007/s11669-024-01090-2

ORIGINAL RESEARCH ARTICLE

Experimental Investigation and Thermodynamic Assessment of the Cr–Ti System

Agustin Flores[1,2] · Sylvie Chatain[1] · Paul Fossati[1] · Frank Stein[3] · Jean-Marc Joubert[2]

Submitted: 13 October 2023 / in revised form: 17 November 2023 / Accepted: 22 December 2023 / Published online: 23 February 2024

Abstract The Cr–Ti system was investigated by several experimental methods and first-principles calculations. The thermodynamic activity of the body-centered cubic solid solution was measured by Knudsen effusion mass spectrometry. The stability of all three polymorphic structures of the Laves phase (*C*14, *C*15, and *C*36) was determined by differential thermal analysis, and the equilibrium tie-lines with the solid solution were obtained by combining results from diffusion couples and equilibrated alloys. The enthalpy of formation of the Laves phases with the corresponding end-members were calculated using density functional theory and the obtained values were integrated in the models. The experimental and computed data available in the literature was reviewed and the binary system was assessed by the Calphad method. The present evaluation results in an improved thermodynamic description, which can describe the experimentally observed activity in a large temperature range. The temperatures of the invariant reactions between the *C*15 and the *C*36 phase with the Cr-rich and the Ti-rich bcc solid solution were significantly modified. The difference of the temperature of transformation between the *C*15 and the *C*36 polytypes on both sides of the Laves phase is much smaller than reported previously.

Keywords activity · Calphad · laves phases · phase diagram

1 Introduction

Chromium and titanium are alloying elements that appear commonly in structural alloys. Cr is known to drastically improve corrosion resistance in steels and other alloys.[1,2] Ti, being a lightweight element, is attractive for applications where the mechanical strength-to-weight ratio is important.[3] The Cr–Ti binary system is also interesting because it is one of the few systems where all three polymorphic structures of the Laves phases, *C*14, *C*15 and *C*36, are stable[4] (Fig. 1). These crystal structures are the most common amongst intermetallic compounds throughout the periodic table, thanks to their high packing density. Laves phases are hard and brittle, which makes them advantageous for some applications, for example as a second phase for precipitation hardening, but of limited use as single-phase, bulk structural materials.[5] The presence of only tetrahedral interstices makes them interesting for solid hydrogen storage.[6,7] Like the face-centered cubic (fcc) and hexagonal close-packed (hcp) structures, which differ in their stacking sequence of atom layers, the difference between the Laves phase polytypes is the stacking order of certain layer packages, each consisting of four atomic

This invited article is part of a special tribute issue of the *Journal of Phase Equilibria and Diffusion* dedicated to the memory of Thaddeus B. "Ted" Massalski. The issue was organized by David E. Laughlin, Carnegie Mellon University; John H. Perepezko, University of Wisconsin–Madison; Wei Xiong, University of Pittsburgh; and *JPED* Editor-in-Chief Ursula Kattner, National Institute of Standards and Technology (NIST).

✉ Jean-Marc Joubert
jean-marc.joubert@cnrs.fr

[1] Service de recherche en Corrosion et Comportement des Matériaux, Université Paris-Saclay, CEA, Gif-Sur-Yvette, France

[2] Université Paris Est Creteil, ICMPE, Thiais, France

[3] Max-Planck-Institut für Eisenforschung GmbH, Düsseldorf, Germany

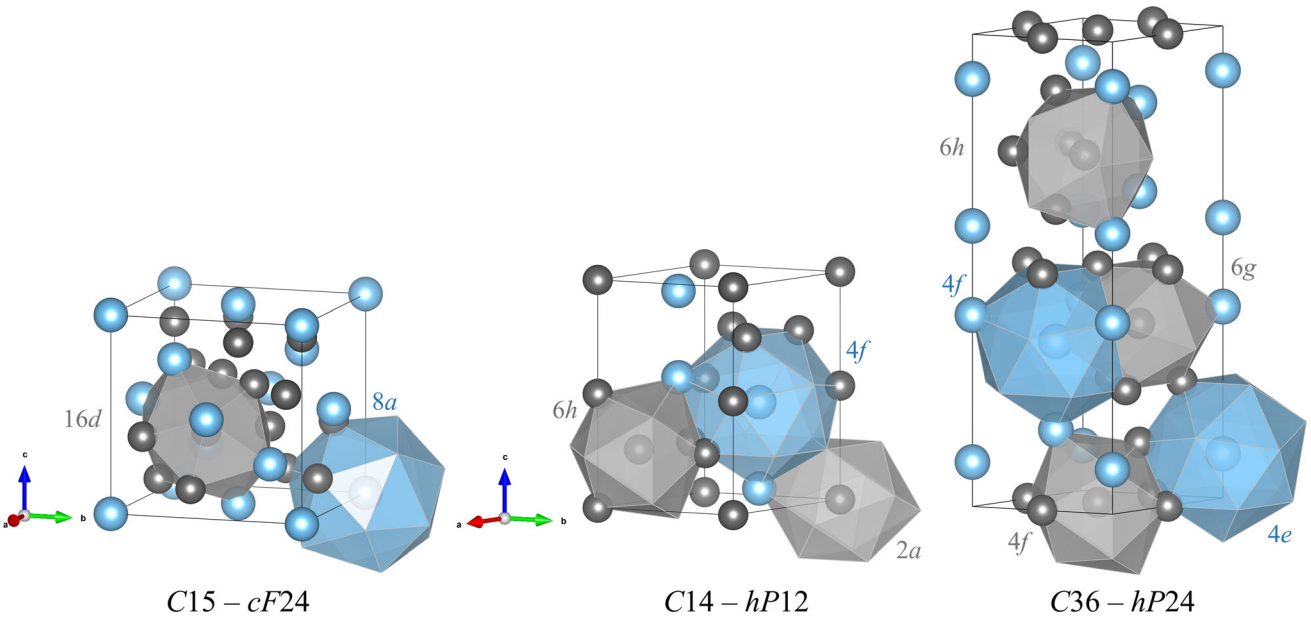

Fig. 1 Crystal structure of Laves phases. The CN16 (grey) and CN12 (blue) polyhedra are highlighted (Color figure online)

layers. Detailed information about the properties and applications of Laves phases can be found elsewhere.[8]

Despite the importance of the Cr–Ti binary system, several discrepancies are found in the phase diagrams and thermochemical properties reported in the literature. Experimentally, both elements tend to react with oxygen and nitrogen leading to the formation of oxide or nitride compounds, which results in inaccurate experimental results. The high volatility of Cr also induces difficulties in the study of high-temperature equilibria and properties, especially in Cr-rich samples. Ti diffusion in the body-centered cubic (bcc) solid solution is several orders of magnitude greater than that of Cr, making it more difficult to reach equilibrium.[9-12] Moreover, the different and sometimes contradictory reports about the crystal structures of the Laves phase make the interpretation of experimental results challenging.

This work tries to clarify the phase diagram of the Cr–Ti system based on new experiments. Diffusion couples and equilibrated alloys were used to determine the tie-lines of equilibrium phases and their solubility limits. Thermal analysis was employed to measure the temperature of invariant reactions. Knudsen effusion mass spectrometry (KEMS) was used to study the properties of the bcc solid solution. In addition, density functional theory (DFT) calculations were carried out to obtain the properties of Laves phases at 0 K. Finally, a thermodynamic assessment using the Calphad approach was performed based on all the previous published data and present results.

2 Literature Review

2.1 Crystal Structure

The Cr–Ti system consists of the liquid, bcc and hcp solid solutions, and three polymorphic Laves phases: $C15$-$TiCr_2$ (cubic $MgCu_2$ structure), $C14$-$TiCr_2$ (hexagonal $MgZn_2$ structure) and $C36$-$TiCr_2$ (hexagonal $MgNi_2$ structure).[13] These phases with their respective crystal structures and the corresponding Calphad sublattices models are listed in Table 1. The Laves phases belong to the group of Frank-Kasper intermetallic phases showing a topologically close-packed (TCP) structure.[14] These structures consist of triangular face coordination shells forming only tetrahedral interstices. The atoms are placed in the center of these polyhedra, surrounded by 16 or 12 neighbors. These sites are designated by their coordination number (CN), CN16 polyhedron and CN12 icosahedron, respectively. The difference between the Laves structures is the stacking order of these close-packed polyhedra. The stability of the Laves phases is mainly controlled by the atom size ratio between the constitutive elements. Their formation is favored when $r_A/r_B \approx 1.225$, reaching a maximum of packing density. These phases have an AB_2 stoichiometry, where A is the bigger atom which is placed on 16 coordinated sites and B is the smaller atom which tends to be placed on 12 coordinated sites. Many Laves phases present a homogeneity domain. Though, in rare cases, the non-stoichiometry may be accommodated by vacancies (mainly in rare-earth based

Table 1 Crystal structure and models of stable phases

Phase	Prototype	Space group	Pearson symbol	Strukturbericht	Model	Wyckoff position (CN)
bcc (Cr, β-Ti)	W	$Im\ \bar{3}\ m$	*cI*2	*A*2	$(Cr,Ti)(Va)_3$	2*a*
hcp (α-Ti)	Mg	$P6_3/mmc$	*hP*2	*A*3	$(Cr,Ti)(Va)_{0.5}$	2*c*
α-$TiCr_2$	$MgCu_2$	$Fd\ \bar{3}\ m$	*cF*24	*C*15	$(Cr,Ti)(Cr,Ti)_2$	[8*a*(16)] ; [16*d*(12)]
β-$TiCr_2$	$MgNi_2$	$P6_3/mmc$	*hP*24	*C*36	$(Cr,Ti)(Cr,Ti)_2$	[4*e*(16), 4*f*(16)] ; [4*f*(12), 6*g*(12), 6*h*(12)]
γ-$TiCr_2$	$MgZn_2$	$P6_3/mmc$	*hP*12	*C*14	$(Cr,Ti)(Cr,Ti)_2$	[4*f*(16)] ; [2*a*(12), 6*h*(12)]

systems), the predominant mechanism for transition metal systems is anti-site atoms (See, Ref [8] 3.2.1 Constitutional point defects). In particular, this has been shown to be the case for the *C*36 phase in the Cr–Ti system.[15]

2.2 Experimental Phase Diagram Data

The crystal structure of solid Cr is bcc. Due to its volatility, considerable discrepancies exist in the literature concerning the value of its melting point.[16,17] Ti has two allotropic structures, hcp at low temperature and bcc above 882 °C, which is stable up to the melting point. The bcc solid solution is stable on both sides of the Cr–Ti phase diagram and there is a small range of temperature where it extends over the entire composition range. In contrast, the solubility of Cr in the hcp phase is very low. In the literature, it is accepted that the three polytypic Laves phases *C*14, *C*15 and *C*36 occur around the $TiCr_2$ stoichiometry. The stability ranges of the Laves phases, in terms of composition and temperature, have been the focus of many investigations. The data are scattered due to the reactivity of Ti and Cr, which both tend to react easily with oxygen and nitrogen. Literature dealing with the experimental determination of the Cr–Ti phase diagram is listed in Table 2.

Vogel and Wenderott[18] investigated for the first time the binary system on the Cr-rich side. They found the presence of an intermetallic compound of unknown structure around 40 at.% Ti (named Cr_3Ti_2). Solidification involving a eutectic reaction was proposed. The very first attempt to determine the whole constitutional phase diagram was carried out by McQuillan.[19] It confirmed the occurrence of an intermetallic compound but at 60 at.% Ti (Ti_3Cr_2 instead of Ti_2Cr_3). It was also found that the bcc structure is stable over the whole composition range between 1360 and 1400 °C. Decomposition of the bcc solid solution in the Ti-rich part of the diagram occurs following a eutectoid reaction, by forming the intermetallic compound and the hcp solid solution. Van Thyne et al.[21], Cuff et al.[22] and Duwez and Taylor[20] performed further studies of the phase diagram and generally agreed with the previous studies. Among them, Duwez and Taylor identified the crystal structure of the intermetallic compound, which corresponds to the prototype Cu_2Mg (*C*15). Levinger[23] showed the existence of a high temperature modification of the $TiCr_2$ compound, the hexagonal *C*14 Laves phase. The phase diagram containing the *C*15 and *C*14 phases was accepted and further studied, several authors investigating invariant reactions and phase boundaries. Svechnikov et al.[4] introduced the *C*36 Laves phase in the Cr–Ti system. The stability, microstructure and mechanical properties of the three Laves phases in this system have been studied in detail by Chen et al..[42-44] Several authors focused on the eutectoid reaction[24-27,30,31,33] and Cr solubility in the hcp structure.[22,25,32,39] In contrast, data related to the solubility of Ti in bcc-Cr remained scarce. There have also been attempts to study the Cr–Ti system using diffusion couples.[45,49,50] There is a general agreement on the solubility on the Ti-rich side of the diagram, but the electron probe microanalysis (EPMA) analyses of the diffusion couples showed a much lower solubility of Ti in bcc-Cr compared to classical optical metallographic investigations on equilibrated alloys.

There are considerable discrepancies in the invariant reactions reported in the literature. There is a consensus concerning both the composition and temperature of the congruent melting of the bcc solid solution. The same is true for the precipitation of the *C*14 phase from the bcc solid solution. However, several authors studied the eutectoid reaction and reported transformation temperatures between 660 and 728 °C. Transformation temperature between different polytypes of Laves phases present an acceptable agreement. The *C*15-*C*36 temperature of transformation in the Cr-rich side was not directly measured by thermal analysis, it was only bounded by the results of Farrar and Margolin[34] for two heat treatments at 800 and 900 °C. Note that the older measurements of invariant reactions were reinterpreted after the *C*36 phase discovery.

2.3 Thermodynamic Data

Pool et al.[36] measured the activity of Cr in the bcc solid solution between 1250 and 1380 °C. Knudsen effusion technique with direct weighing of the cell was used. It was made possible by neglecting the contribution of Ti, which was justified by the large difference between the vapor

Table 2 Compiled list of literature dealing with the phase diagram and thermochemical data of the Cr–Ti system

Reference	Year	Experimental technique	Studied range/Property	Used
Vogel [18]	1940	Metallography, thermal analysis	0-60 at.% Ti, Ti_3Cr_2	No
McQuillan [19]	1951	Metallography, XRD, incipient melting	Whole system, Ti_2Cr_3	Yes
Duwez [20]	1952	Metallography, XRD	Eutectoid, $TiCr_2$ (*C*15)	Yes
Van Thyne [21]	1952	Metallography, XRD, incipient melting, thermal analysis	25-100 at.% Ti	Yes
Cuff [22]	1952	Metallography, dilatometry, XRD, hardness	Whole system	Yes
Levinger [23]	1953	Metallography, XRD	$TiCr_2$ (*C*14)	Yes
McQuillan [24]	1954	H pressure, Metallography	Eutectoid	No
Kornilov [25]	1957	Metallography, resistivity, thermal analysis, hardness	Whole system	Yes
Bagariatskii [26]	1958	Metallography	Eutectoid	Yes
Goldenstein [27]	1959	Metallography	Eutectoid	Yes
Gross [28]	1960	Metallography, XRD	$TiCr_2$ (*C*14 and *C*15)	Yes
Ageev [29]	1961	Metallography, XRD	Eutectoid	Yes
Ermanis [30]	1961	Metallography, XRD	Eutectoid	Yes
Mikheyev [31]	1962	Resistivity	Eutectoid	Yes
Mikheyev [32]	1962	Hardness	Cr solubility in hcp	No
Svechnikov [33]	1962	DTA, Dilatometry, XRD	Whole system	Yes
Farrar [34]	1963	Metallography, XRD	0-60 at.% Ti	Yes
Ageev [35]	1963	XRD	Ti solubility in bcc	Yes
Pool [36]	1967	Knudsen-effusion cell	Activity of Cr	No
Rudy [37]	1969	Incipient melting	Solidus	Yes
Svechnikov [4]	1970	Metallography, thermal analysis, XRD	25-40 at.% Ti, $TiCr_2$ (*C*36)	Yes
Minayeva [38]	1971	Metallography, thermal analysis, XRD	20-75 at.% Ti	Yes
Faudot [39]	1984	Resistivity	Cr solubility in hcp	Yes
Kudielka [40]	1990	Metallography, XRD, EPMA	Tie-lines $TiCr_2$-bcc	Yes
Sluiter [41]	1991	Tight-binding CPA-GPM	bcc mixing enthalpy, $TiCr_2$ Formation enthalpy	No
Chen [42]	1994	XRD, EPMA	Laves phases stability	No
Chen [43]	1997	Metallography, XRD, EPMA	Tie-lines $TiCr_2$-bcc	Yes
Chen [44]	1998	XRD, EPMA	Laves phases stability	No
Zhuang [17]	2000	XRD	30, 40, 50 at.% Ti; 1000 °C	No
Zhao [45]	2004	EPMA (diffusion multiple)	1000-1200 °C	No
Baumann [46]	2011	Thermal analysis, XRD, EPMA	$TiCr_2$ (*C*36 and *C*14)	Yes
Chandran [47]	2013	SQS-DFT	bcc mixing enthalpy	No
Sahara [48]	2015	SQS-DFT	bcc mixing enthalpy	No
Zhu [49]	2017	EPMA (diffusion multiple)	800-1200 °C	Yes
Xu [50]	2020	EPMA (diffusion multiple)	1000 °C	No

Last column refers to whether the reference was considered during optimization.

pressure of the two pure elements. Their results indicate a strong influence of the temperature on the activity, and a very high positive enthalpy of mixing. Ohsaka et al.[51] measured heat of fusion and the enthalpy increment of the solid and liquid phase for a 60 at.% Ti alloy. The alloy melted congruently at 1415 ± 10 °C.

The Cr–Ti system was also studied using different calculation methods. Several calculations were performed to obtain thermodynamic quantities, both for the solid solutions and the Laves phases. Sluiter and Turchi[41] studied the system using the coherent-potential approximation (CPA) and generalized perturbation method (GPM) within the tight–binding framework. They concluded that mixing is favored and predict an ordered phase with a *B*2-CsCl structure. Crivello,[52] Chandran et al.[47] and Sahara et al.[48] obtained the enthalpy of mixing in the bcc solid solution using the special quasi-random structure (SQS) method. The results show large discrepancies between the different authors, from largely positive to negative values. Pavlů et al.[53] calculated the enthalpy of formation of all

the end-members of the Laves phases using electronic structure calculations based on the DFT. Sluiter[54] computed the lattice stability of the pure elements in the *C*14 and *C*15 Laves phases structures. Chen et al.[55] calculated the enthalpy of formation of the stable configuration of Laves phases by the same method. First principles calculations of stable and metastable ordered Laves phase show an excellent agreement between them. Unfortunately, there are no experimental data to validate such calculations.

Thermodynamic modeling of the Cr–Ti binary system has been approached repeatedly as new experiments demonstrated the presence of different allotropic structures of the $TiCr_2$ intermetallic phase. Kaufman and Nesor[56] have assessed the system for the very first time. They considered a single stoichiometric compound at $TiCr_2$ composition. Then, Saunders in the COST 507[57] project reassessed the system differentiating the cubic Laves phase (*C*15) from the hexagonal one (*C*14). The improvement introduced by Saunders was not only the independent modeling of these two phases, but also the modeling of the non-stoichiometric character of the Laves phases. Lee et al.[58] introduced the modeling of the third Laves phase, *C*36, preserving a simplified two-sublattice model similar to Saunders's. Since this evaluation, different models were proposed. Several authors kept this model and others chose to model the hexagonal phases with more than two sublattices. Chronologically, Zhuang et al.,[17] Ghosh,[59] Pavlů et al.,[53] Cupid et al.[60] and Sun et al.[61] re-assessed the system.

3 Techniques and Methods

3.1 Sample Preparation

High purity elements were supplied by Goodfellow, Cr (99.9%) and Ti (99.999%), and Sigma Aldrich, Cr (99.995%) and Ti (99.99%). Alloys were prepared by arc melting under high purity argon using a non-consumable tungsten electrode. To capture all residual nitrogen and oxygen in the chamber, pure Ti or zirconium was melted several seconds before alloy casting. Alloys were re-melted several times by flipping the samples to ensure homogeneity, and some of them were inspected by x-ray tomography to detect the presence of unmelted Cr. The chemical compositions of the as-cast samples were obtained recalculating the composition by a mass balance, if the weight loss comes from Cr evaporation. Nevertheless, weight loss during melting was less than 1 wt.%. The composition was verified by scanning electron microscopy using the x-ray energy dispersive spectroscopy (SEM-EDS) technique or by electron probe micro analysis using the x-ray wavelength dispersive spectroscopy (EPMA-WDS) technique.

3.2 Phase Diagram Determination

The Cr–Ti phase diagram was studied by diffusion couples and equilibrated alloys. A list of samples and the treatment conditions, temperature, time, and composition are shown in Table 3.

Diffusion couples were made to determine the solubility range of each phase at the heat-treatment temperature. Pure Cr and Ti were used to map the entire composition space. In addition, two-phase alloys were cast with compositions on both sides of the Laves phases, where such phases are expected to be in equilibrium with the bcc solid solution. The selected nominal compositions were 24, 48 and 62 at.% Ti. Thus, the composition and crystal structure of the Laves phases and the solid solution can be obtained. To characterize the alloys, EDS and WDS techniques were employed to measure the chemical composition and Rietveld refinement was used on powder x-ray diffraction (XRD) patterns to determine the crystal structure.[62] These samples were also employed to determine the invariant reactions by differential thermal analysis (DTA).

Heat treatments of samples were carried out in a tubular resistance furnace. In preliminary studies, it was evidenced that the transformation between the different polytypes of the Laves phases in the Cr-rich side was very sluggish. To avoid equilibration problems, the 24 at.% Ti alloy was subjected to a homogenization treatment at 1300 °C for 12 h followed by water quenching. This treatment allowed us to obtain a homogeneous bcc solid solution. To achieve this temperature without introducing any contamination, the samples were sealed under high purity Ar into pure molybdenum crucibles. These samples and as cast 48 and 62 at.% Ti samples were wrapped in tantalum foil and treated in argon-refilled sealed quartz ampoules. For temperatures above 1100 °C, metallic Ti was added as an oxygen and nitrogen getter. High temperature microstructures were retained for subsequent characterization at room temperature by water quenching after heat treatments. A fraction of these samples, as well as as-cast samples were used for DTA. In addition, two samples have been cast at 30 and 40 at.% Ti to increase the volume fraction of the Laves phases and consequently improve the signal related to thermal arrests. These analyses were done in a Setaram SETSYS 1600 that was calibrated by melting pure elements Ni, Ag, and Au. Crucibles were chosen depending on the temperature reached. For high temperatures, Y_2O_{3-x} acts as an oxygen getter and does not react with alloy melts.[63] For solid reactions, Al_2O_3 was used instead. Different heating and cooling rates between 1 and

Table 3 List of samples with experimental conditions and EPMA results of each phase boundary

Id.	Method	Composition	Temperature, °C	Time, h	bcc (Cr-rich)	Laves (Cr-rich)	Laves (Ti-rich)	bcc (Ti-rich)
DC-900	Diffusion couple	Cr/Ti	900	1440	1.6	33.4	36.2	78.6
DC-1000	Diffusion couple	Cr/Ti	1000	720	2.8	34.7	37.2	71.4
DC-1100	Diffusion couple	Cr/Ti	1100	540	3.2	33.1	36.7	64.7
DC-1200	Diffusion couple	Cr/Ti	1200	144	11.5	32.7	36.4	60.8
EA-24	Equilibrated alloy	23.6	750	2160	…	33.3		
			900	1440	…	32.9		
			1000	720	10.6	33.6		
			1100	540	11.6	33.0		
EA-48	Equilibrated alloy	48	900	1440			35.1	78.7
			1000	720			36.6	71.1
			1100	540			36.2	64.9
			1150	360			36.2	63.7
EA-62	Equilibrated alloy	61.9	900	1440			35.5	78.7
			1000	720			35.6	71.0
			1100	540			36.2	66.1

Chemical composition are expressed in at.% Ti.

10 K/min were used to extrapolate the invariant reactions to equilibrium conditions with a zero heating rate.

Diffusion couples were prepared by putting together ground and polished pieces ($5 \times 5 \times 10$ mm^3) of the pure metals Cr and Ti. The diffusion couple was put into a small, closed alumina crucible which was wrapped with Ta foil. The crucible was inserted upside down into a larger alumina crucible and the space between the two crucibles was filled with fine chips of Ti as getter material. The heat treatment and quenching methodology was the same as for the equilibrated alloys. The chemical composition profiles of the diffusion interphase were obtained by EPMA done in a Jeol JXA-8100 microprobe, and the XRD patterns were acquired in a Bruker D8 using Cu Kα radiation.

3.3 Thermodynamic Activity Measurements

The description of the apparatus and the method can be found elsewhere.[64-66] The mass spectrometer used in this work is a XBS quadrupole 510 series constructed by Hyden Analytical. When a condensed alloy is in thermodynamic equilibrium with its gaseous phase, the activity (a_i) of an element i in the alloy can be defined as the ratio of the partial vapor pressure of i (P_i) to the vapor pressure of the pure element (P_i^o), at the same temperature (1).

$$a_i = \frac{P_i}{P_i^o} \quad \text{(Eq 1)}$$

$$P_i = \frac{I_i^+ . T}{S_i} \quad \text{(Eq 2)}$$

Applying this equation, gaseous phases are considered as ideal gases, which is reasonable for low pressure.[67] Effused species from the Knudsen cell are ionized by electron collisions. The partial pressure P_i is obtained from the relation (2) by measuring the ionic current (I_i^+) with a mass spectrometer. In this equation, T is the temperature of the sample and S_i is the sensitivity, a factor that depends on the species i, the ionization cross-section, the isotopic abundance, and a geometrical factor. For activities measurements, a multiple Knudsen cell-mass spectrometric assembly was used. In a multiple cell, we usually reserve a cell for a reference, in this case one of the pure elements, and the others for the alloys. The main advantage of this set-up is that the sensitivity remains constant between two Knudsen cells for the same element. Thus, the thermodynamic activity at a given temperature is obtained by the ratio between the ionic current of the element in the alloy and the reference. A restricted collimation configuration was used to discard the detection of the parasitic surface re-vaporization.

The vapor species were ionized with an electron emission current of 0.3 mA and an acceleration potential of 15 eV. The whole system, ionization chamber, furnace chamber and spectrometer, reached ultra-high vacuum better than 5×10^{-8} mbar (5×10^{-6} Pa). Cr can be found in four stable isotopes, ^{52}Cr being the most abundant (83.79%). For this reason, the spectrometer was configured to acquire information only from this isotope. Temperature was measured by a bi-chromatic Impac optical pyrometer, which was calibrated by melting pure elements Ag, Au,

and Fe at low temperatures and the well-known eutectic reaction of Ru–C at high temperature. Different crucibles materials were tested before choosing sub-stoichiometric yttrium oxide (Y_2O_{3-x}). Alumina and boron nitride reacted with samples, especially during melting. The Knudsen cells, crucibles, each one with a lid containing a 2 mm diameter effusion hole, were placed in a tantalum cell-block support. The cell-block containing the samples was subjected to an isothermal treatment of 1 h around 1380 °C before data acquisition in order to homogenize the bcc solid solution.

Our work was restricted to the study of the Ti-rich region to limit shifts of the composition caused by Cr evaporation. In addition, only single-phase fields were addressed in order to avoid kinetic and equilibration issues during formation or dissolution of the Laves phases. The temperature domain is also limited by physical phenomena inherent of this technique. The lowest accessible temperature is dictated by the detection limit of the mass spectrometer and the highest temperature is limited by a transition from free molecular flow to a collisional regime.

3.4 DFT Calculations

First principles calculations are a powerful tool to generate input data for Calphad assessments.[68] They can be used to estimate thermodynamic properties of stable and metastable phases such as enthalpy of formation and temperature-dependent heat capacity and entropy. In the Calphad formalism, it is often necessary to fix the enthalpy of formation of several metastable phases. These values cannot be directly measured experimentally, but they can be obtained with such calculations.

DFT calculations were performed using the Vienna Ab-initio simulation package (VASP)[69,70] and the projector augmented wave (PAW) method.[71] The exchange-correlation energy of electrons was described in the generalized gradient approximation (GGA) using the functional parametrization of Perdew–Burke–Ernzerhof (PBE).[72] Input files and relaxation routines were set-up with the open source code ZenGen.[73] This code generates all the initial structures, which can be used to perform a systematic relaxation of all the possible combinations of crystal structures and element distributions on each lattice site. A four-step relaxation was performed to reduce the calculation time and ensure convergence. In the first relaxation step, only the volume was allowed to change, whilst the shape of the simulation box and the ionic positions were kept fixed. In the second step, the box shape constraint was released. In the third step, the ionic positions were relaxed, and all the cell parameters and internal degrees of freedom were allowed to change to reach the ground state. Finally, full relaxation with stronger convergence criteria and a much finer k-point grid were performed to obtain properties of interest. Geometrical relaxation was considered as converged when the total energy difference between two successive iterations varies less than 10^{-4} eV for the three first steps and 10^{-5} eV for the last step. For the cubic $C15$ phase, a $8 \times 8 \times 8$ Monkhorst–Pack[74] k-point grid was used for the initial steps and a $16 \times 16 \times 16$ grid for the last step. For the hexagonal $C14$ and $C36$ phases, the calculations were started using an $8 \times 8 \times 5$ grid and a $16 \times 16 \times 10$ grid for the last relaxation was used instead. The cut-off energy was set to 400 eV.

4 CALPHAD Modeling

In the Calphad method, the equilibrium state of a system subjected to finite conditions can be obtained by the minimization of the Gibbs energy of the phases. The reference states adopted for this work are those proposed by Scientific Group Thermodata Europe (SGTE) in their last version (2009) of the Unary database.[75]

The liquid phase and solid solutions were modeled with a disordered substitutional solution model, which treats each element randomly distributed in the phase. The molar Gibbs energy G^{φ} of the phase φ is

$$G^{\varphi} = \sum_{i=\mathrm{Cr,Ti}} x_i G_i^{\varphi} + RT \sum_{i=\mathrm{Cr,Ti}} x_i \ln(x_i^{\varphi}) + x_{\mathrm{Cr}} x_{\mathrm{Ti}} \sum_{v} {}^{v}L_{\mathrm{Cr,Ti}}^{\varphi} (x_{\mathrm{Cr}} - x_{\mathrm{Ti}})^{v} \quad \text{(Eq 3)}$$

where x_i denotes the mole fraction of the component i, G_i^{φ} is the molar Gibbs energy of the pure element i in the phase φ. The three terms in this expression are the mechanical mixing contribution, the contribution of the ideal configurational entropy, and the excess Gibbs energy, which is represented by $L_{Cr,Ti}^{\varphi}$. The excess term is described with a Redlich-Kister expression. The interaction parameter L is

$${}^{0}L_{\mathrm{Cr,Ti}}^{\varphi} = A + B.T$$

$${}^{1}L_{\mathrm{Cr,Ti}}^{\varphi} = C + D.T$$

$${}^{2}L_{\mathrm{Cr,Ti}}^{\varphi} = E + F.T$$

where A, B, C, D, E and F are the optimized parameters.

The Laves phases ($C15$, $C14$ and $C36$) were modeled using a simplified two-sublattice model under the compound energy formalism (CEF). Since the solubility of such phases is limited, evidenced by a narrow stability domain, only little mixing occurs in the different sites. Baumann and Leineweber[15] performed structure refinements of the $C36$ Laves phase concluding that the off-stoichiometry is the product of anti-site defects, by Ti atoms occupying Cr sites. In addition, site occupancies of

the different CN12 sites were essentially the same. In the adopted two-sublattice model, there is one sublattice for the CN16 sites and a second one for the CN12 sites. In addition, Cr and Ti are allowed to occupy both sublattices, to accommodate off-stoichiometry by antisite defects on both sides. The resulting model is expressed as $(Cr,Ti)(Cr,Ti)_2$, and the molar Gibbs energy is

$$G^{\varphi} = \sum_{i=Cr,Ti}\sum_{j=Cr,Ti} y_i^I y_j^{II} G_{i:j}^{\varphi} + RT\left[\sum_{i=Cr,Ti} y_i^I \ln\left(y_i^I\right) + 2\sum_{j=Cr,Ti} y_j^{II}\ln\left(y_j^{II}\right)\right] + {}^{ex}G^{\varphi} \quad \text{(Eq 4)}$$

In this case, mixing occurs and is defined independently in both sublattices. This is represented by the variables, y_i^I and y_i^{II}, which are the site fractions of the element i in the first and second sublattice, respectively. The same formalism is applied to the element j.

Excess enthalpy ${}^{ex}G^{\varphi}$ is expressed for each sublattice. Thus, we can define four interaction parameters. If the interaction occurs on the first sublattice I as $(A,B)(A)_2$ and $(A,B)(B)_2$ we can define the excess term as follows.

$${}^{ex}G^{\varphi} = \sum_{i=A,B} y_i^{II} y_A^I y_B^I \sum_{v} {}^{v}L_{A,B:i}^{\varphi}\left(y_A^I - y_B^I\right)^v$$

By contrast, if the interaction occurs on the second sublattice II as $(A)(A,B)_2$ and $(B)(A,B)_2$ we can define the excess term

$${}^{ex}G^{\varphi} = \sum_{i=A,B} y_i^{I} y_A^{II} y_B^{II} \sum_{v} {}^{v}L_{i:A,B}^{\varphi}\left(y_A^{II} - y_B^{II}\right)^v$$

We will consider during the optimization that the interaction within a site is not affected by the occupancy of the other site, thus $L_{A,B:A}^{\varphi} = L_{A,B:B}^{\varphi}$ and $L_{A:A,B}^{\varphi} = L_{B:A,B}^{\varphi}$.

5 Experimental and Calculated Results

5.1 Phase Diagram

Diffusion couples show the presence of $TiCr_2$ intermetallic compound at the interface, as can be seen in Fig. 2. The solubility of Cr in β-Ti is in agreement with previous works,[30] while the solubility of Ti in Cr between 900 and 1100 °C is significantly lower than expected from the accepted phase diagram, similar to what was found in previous works.[49,50] Characteristic composition profiles as obtained from EPMA scans of the diffusion couples after annealing at 900, 1000 and 1100 °C are shown in Fig. 3. To improve statistics and decrease uncertainty, between 3 and 10 profiles were analyzed for each diffusion couple.

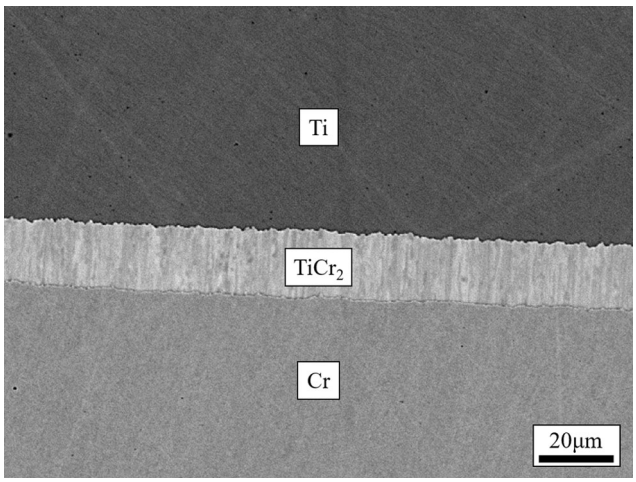

Fig. 2 Backscattered electron image of the Cr–Ti diffusion couple annealed at 1000 °C showing the formation of the $TiCr_2$ intermetallic compound

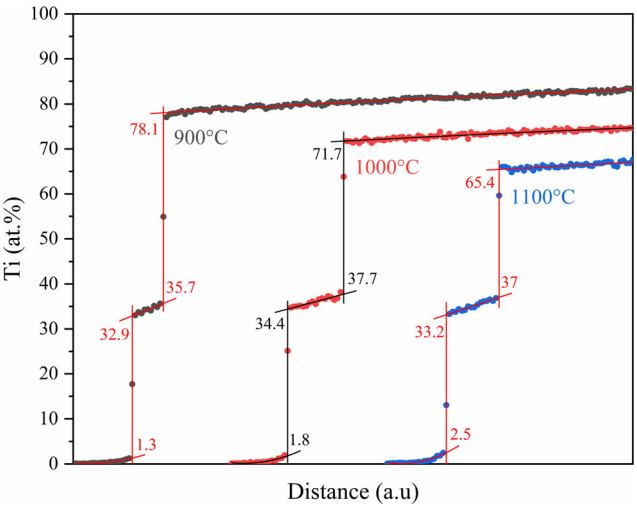

Fig. 3 Composition profiles of diffusion couples obtained at 900, 1000 and 1100 °C

Concerning the equilibrated alloys, the measured tie-lines between Laves phases and the bcc solid solution on the Ti-rich side agree well with the diffusion couples and previous data. On the Cr-rich side, the microstructures were found to be too fine to be measured by EPMA. In order to estimate the solubility limit of the solid solution, Vegard's law was applied. It was first verified from the literature[20,22,37,43,76] that the lattice parameter changes linearly as a function of composition in this system (Fig. 4). Calculations from Sluiter and Turchi[41] and Crivello[52] also confirm this trend at 0 K. The composition of the solid solutions was thus deduced from the lattice parameter obtained from the Rietveld refinement. On the Cr-rich side, equilibrium occurs between the solid solution and the *C*15 phase up to 1150 °C. On the Ti-rich side, tie-lines of these

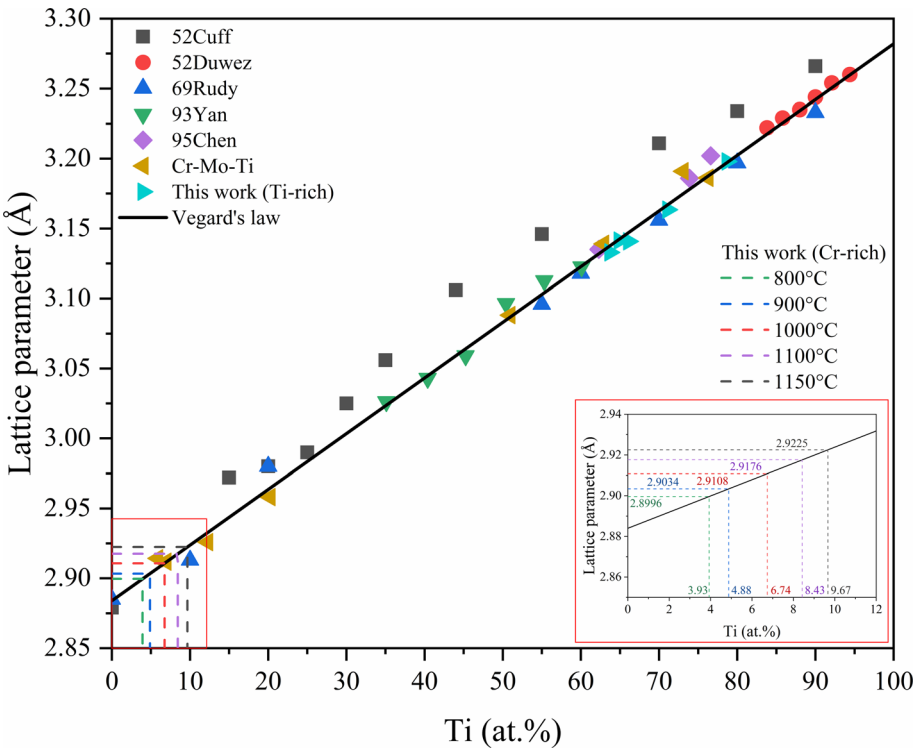

Fig. 4 Lattice parameter evolution of the bcc solid solution as a function of composition. Experimental data[20,22,37,43,75,81].

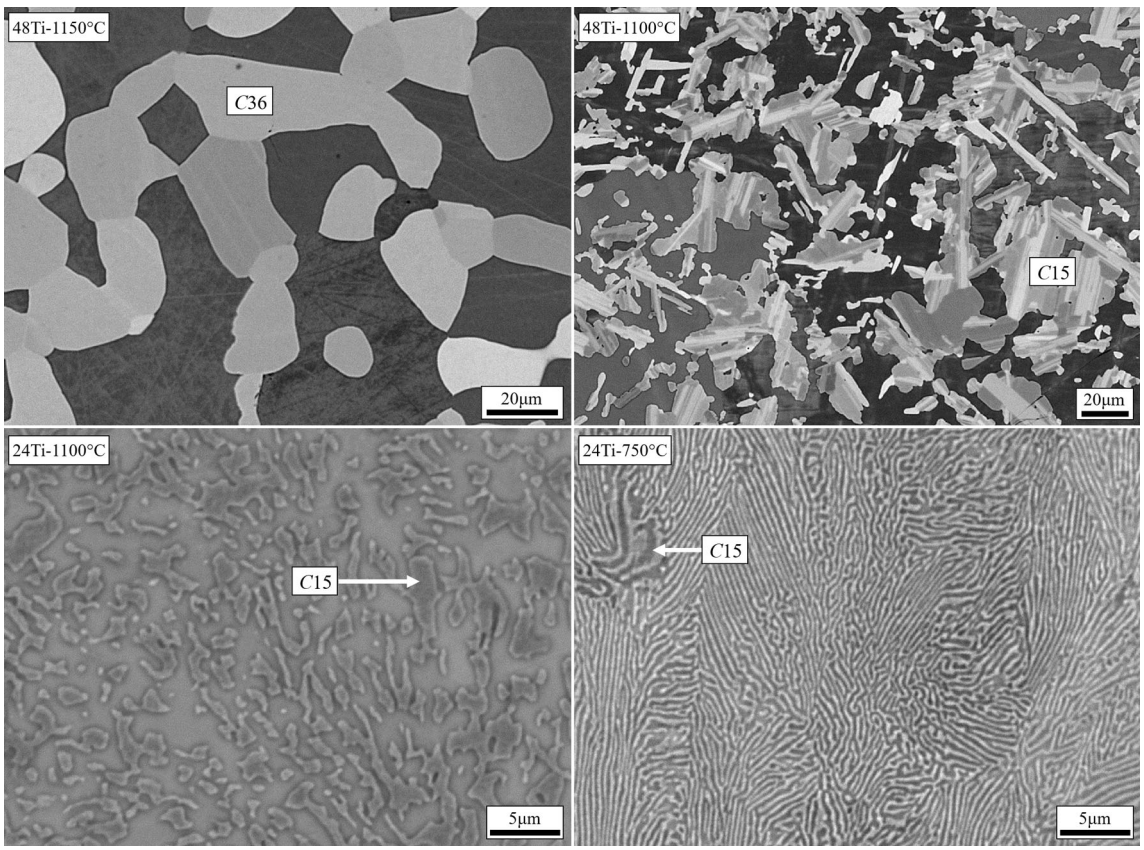

Fig. 5 Backscattered electron images of different heat-treated alloys. Samples containing 48 at.% Ti show the *C*36 Laves phase at 1150 °C and the *C*15 variant at 1100 °C in equilibrium with the bcc solid solution (top). In the case of the alloy with 24 at.% Ti, the microstructure consists of *C*15 and bcc solid solution at 1100 and 750 °C (bottom)

Table 4 List of experimentally determined invariant reaction temperatures in the Cr–Ti system

Invariant reaction	Temperature, °C	Reference	Comment
Liquid → bcc	1400	McQuillan [19]	
	1380	Van Thyne [21]	
	1400	Cuff [22]	
	1400	Kornilov [25]	
	1412 ± 5	Rudy [37]	
	1415 ± 10	Ohsaka [51]	
bcc → *C*14	1360	McQuillan [19]	
	1350	Van Thyne [21]	
	1350	Cuff [22]	
	1365 ± 10	Farrar [34]	
	1360	Svechnikov [4]	
	1375	Baumann [77]	
*C*14 → bcc + *C*36 (Cr-rich)*	1260 ± 20	Svechnikov [4]	Attributed to Ti_3Cr_3O formation
	1272,5 ± 2,5	Minayeva [38]	
	1277	Baumann [46]	
	1272 ± 5	This work	
*C*14 → bcc + *C*36 (Ti-rich)*	1260 ± 20	Svechnikov [4]	Attributed to Ti_3Cr_3O formation
	1272.5 ± 2.5	Minayeva [38]	
	1269	Baumann [46]	
	1257 ± 5	This work	
bcc + *C*36 → *C*15 (Cr-rich)*	850 ± 50	Farrar [34]	Attributed to C14 → bcc + C15 reaction
bcc + C36 → *C*15 (Ti-rich)*	1157,5 ± 7,5	Gross [28]	Attributed to bcc + C14 → C15 reaction
	1150 ± 5	Farrar [34]	Attributed to bcc + C14 → C15 reaction
	1195 ± 10	Svechnikov [4]	
	1225 ± 10	Minayeva [38]	Attributed to bcc + C14 → C15 reaction
	1143 ± 10	This work	
bcc → hcp + *C*15	685	Van Thyne [21]	
	670	Cuff [22]	
	662.5 ± 12.5	Duwez [20]	
	728 ± 10	Kornilov [25]	
	670 ± 5	Goldenstein [27]	
	667 ± 10	Ermanis [30]	
	700 ± 15	Mikheyev [31]	
	662 ± 5	This work	

*Written as obtained from the present thermodynamic calculations.

phases were found up to 1100 °C, while at 1150 °C, the stable Laves phase was found to be *C*36. Figure 5 shows some characteristic microstructures of two-phase alloys obtained in this work.

Thermal analysis was used to define more accurately the temperature of phase transformations. The invariant reaction temperatures obtained by the present DTA investigations are given in Table 4. It should be mentioned that the transformation from *C*15 to *C*36 yields only very weak signals. This was expected, since the energy difference between the two Laves phase variants is very small. Therefore, it was detected only where the phase fraction of Laves phase was high enough. On the Cr-rich side of the Laves phase, the only reaction detected was the *C*36 to *C*14 transformation.

5.2 Thermodynamic Activity Measurement

Activity measurements of Cr in the bcc solid solution are shown in Fig. 6. We found for each composition a positive deviation from ideality, which are drawn by the different dotted lines.

5.3 DFT Calculations

The enthalpies of formation at 0 K for the Laves phase end-members are listed in Table 5 compared with calculated literature data. These energies are in good agreement with literature. According to these calculations, the cubic *C*15 variant is the ground state Laves phase, followed by *C*36 and *C*14, respectively.

6 Discussion and Thermodynamic Assessment

The first phase assessed during optimization was the bcc solid solution because it is the only phase for which we have experimental thermochemical data. The present activity measurements show a positive deviation from ideality in agreement with Pool et al.[36] Temperature has no major effect on the activity, in contrast with the results of these authors. The alumina crucibles used by Pool et al. could have reacted with Ti and formed volatile species. With this reaction, the Cr weight loss could be overestimated resulting in larger values for the activity. This hypothesis was firstly enunciated by Gros et al.[78] Also, Zhuang et al.[17] showed that optimizing the system with all the activity values from Pool, leads to unrealistic parameters. Therefore, our results were considered for modeling the bcc solid solution. Figure 7 shows the experimental data and our model compared to previous assessments. Calculated mixing enthalpies from the literature[41,47,48,52] were not used due to their inconsistency. The enthalpies of mixing from our calculations, presented in Fig. 8, show an acceptable agreement with data from Crivello[52] on the Cr-rich side of the binary system. At high Ti compositions, the mixing enthalpies should converge to zero contrary to what is observed. This is attributed to the fact that the bcc structure becomes mechanically unstable close to pure Ti, so the DFT results cannot be fully trusted in this region.[79,80]

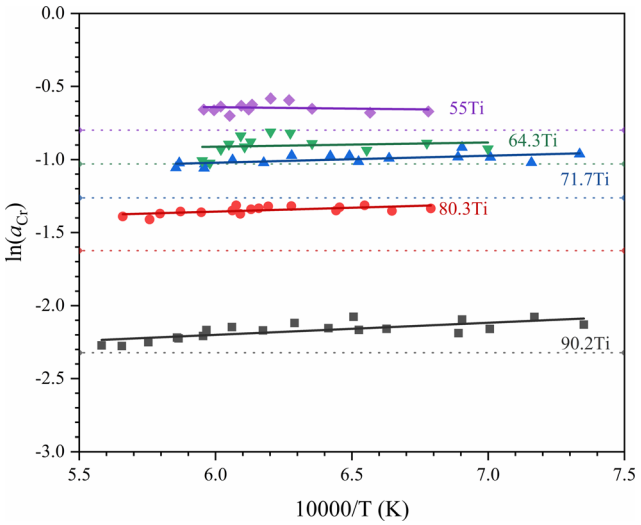

Fig. 6 Napierian logarithm of Cr activity in different alloys as a function of temperature. Reference state is solid Cr and dotted lines represents an ideal mixing behavior

Then, parameters of the liquid phase were optimized with solidus and liquidus data. As it can be seen in Fig. 9, the number of available data on the Ti-rich side is scarce, and values on the Cr-rich side of the phase diagram strongly scatter. As it was mentioned before, Cr volatility could make measurements difficult or inaccurate. Close to the melting point, and especially in Cr-rich samples, composition shifts towards Ti could happen after long high-temperature heat treatments or melting. The results of Kornilov et al.[25] were not taken into account due to their difference to other data. The agreement between data published by Svechnikov et al.,[33] Rudy[37] and Minayeva et al.[38] is good, and for this reason a high weight factor was applied to them during optimization. Temperature and composition of the congruent melting point of the bcc solid solution obtained here was 1408 °C and 57.4 at.% Ti,

Table 5 Calculated enthalpy of formation at 0 K compared with previous calculations (values are in J/mol.at)

Phase	$CrCr_2$	$TiCr_2$	$CrTi_2$	$TiTi_2$	Reference
C15	27179	− 10245	52151	24234	This work
	27089	− 11451	57711	24810	Sun [61]
	27290	− 10160	57270	32260	Pavlů [53]
	26400[1]	− 11967[2]	…	22770[1]	[1]Sluiter [54]/[2]Chen [55]
C14	28531	− 8542	51307	23470	This work
	26463	− 9867	52299	24231	Sun [61]
	28630	− 8470	51390	27200	Pavlů [53]
	27800[1]	− 10200[2]	…	21670[1]	[1]Sluiter [54]/[2]Chen [55]
C36	27650	− 9596	53468	28739	This work
	27559	− 10880	54345	28996	Sun [61]
	27750	− 9510	53530	28360	Pavlů [53]
	…	− 11000	…	…	Chen [55]

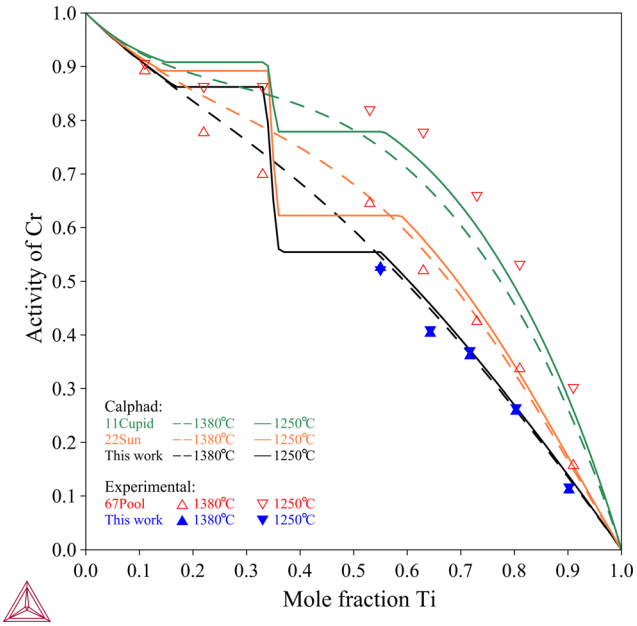

Fig. 7 Calculated activity of Cr compared with previous assessments and experimental data[36,60,61]

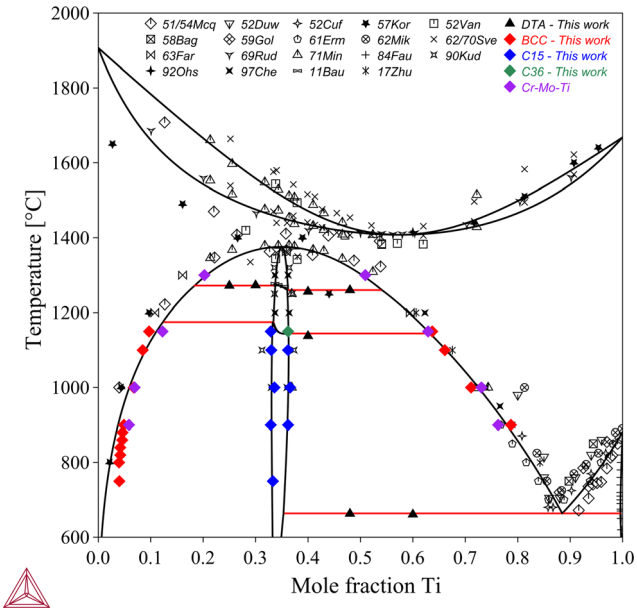

Fig. 9 Calculated phase diagram compared with experimental data[4,19-22,24-27,30,31,33,34,37-40,43,46,49,51]

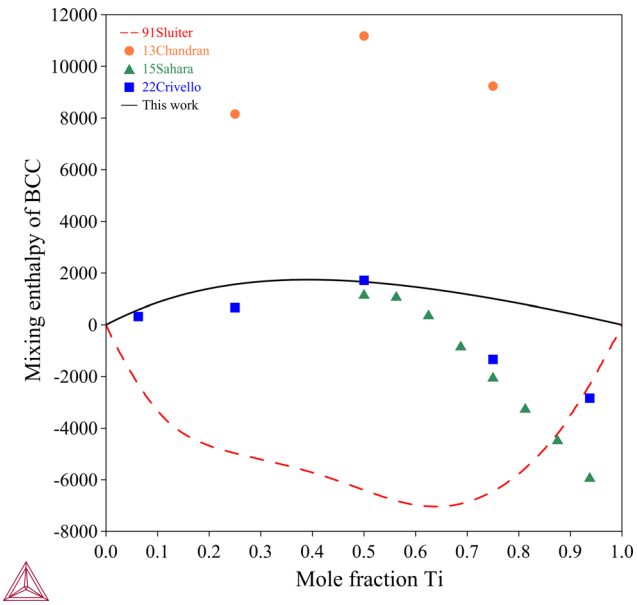

Fig. 8 Calculated mixing enthalpy of the bcc solid solution compared with literature calculated data[41,47,48,52]

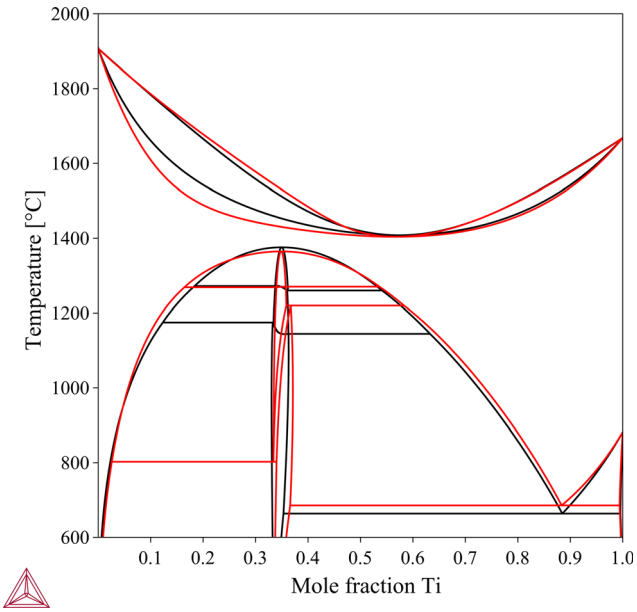

Fig. 10 Comparison of the phase diagram obtained in the current work (black) and the assessments of Cupid et al.[60](red) (Color figure online)

respectively, in good agreement with Ohsaka et al.[51] and Rudy[37] (see Table 4).

To assess the stability of the Laves phases, formation enthalpies were adopted "as-calculated" from our DFT calculations. If there are no standardized lattice stabilities for pure elements for such phases, we choose our results to model all the end-members. Stability at finite temperatures was fitted by the entropy term, and the solubility domain with the interaction parameters.

In the present study, the *C*15 phase is the only stable Laves phase up to 1100 °C, in contrast to the findings of Farrar and Margolin,[34] Minaeva et al.,[38] Svechnikov et al.,[4] and Chen et al.[43] who observed different Laves phases on the two sides of the homogeneity domain. Our results agree with the occurrence of the *C*15 phase on the Ti-rich side. The disagreement appears in the Cr-rich side. The first two studies[34,38] found the *C*14 while in the

Table 6 Computed invariant reaction temperatures compared with data from previous works and selected experimental data

Invariant reaction	Pavlů [53]	Cupid [60]	Sun [61]	Experimental	This work
Liquid → bcc	1433	1404	1436	1412 [37]	1408
bcc → *C*14	1356	1365	1351	1375 [77]	1376
*C*14 → bcc + *C*36 (Cr-rich)	1280	1269	1278	1272	1272
*C*14 → bcc + *C*36 (Ti-rich)	1282	1270	1275	1257	1260
bcc + *C*36 → *C*15 (Cr-rich)	809	803	811	Above 1150 (This work) Below 1200 [46]	1175
bcc + *C*36 → *C*15 (Ti-rich)	1227	1220	1216	1143	1145
bcc → *C*15 + hcp	692	686	698	662	664

two latter studies[4,43] the *C*36 phase was observed. This is explained by a sluggish transformation of either *C*14 or *C*36, formed in as cast samples, to the *C*15 phase. Such a slow and progressive transformation of *C*36 and *C*14 into *C*15 was observed in (Refs [43, 28] respectively.

In the present study, the transition temperature between *C*36 and *C*14 was obtained by DTA. This reaction was evaluated at two different compositions on each side of the Laves phases with an excellent agreement between the two measurements. For each sample, three heating rates were used in order to extrapolate to the equilibrium state, which means a zero heating rate (see "Supplementary information"). The starting temperature of the *C*36-*C*14 reaction was consistent across the different runs. On the contrary, the transition that involves the *C*15 and *C*36 phases on the Ti-rich side shows a difference depending on the heating rate. This difference could be attributed to thermal activation, since at high temperature, equilibrium is attained more rapidly than at lower temperatures.

If we compare the Cr–Ti system with an analogous system, such as Cr–Zr,[13] we find on both phase diagrams the same order of occurrence of the three Laves phases as a function of temperature. The transition between different polytypic structures occurs almost isothermally in both systems.

Diffusion couples and equilibrated alloys were used to investigate the solubility of phases and equilibrium tie-lines. A good agreement between both techniques was generally found for the solubility of Cr in β-Ti. In contrast, the determination of the solubility of Ti in Cr raises difficulties. The values obtained with diffusion couples are lower than those from equilibrated samples. The same effect was also observed in the Hf–Ti system by Zhu et al.[49] The difference could be attributed to kinetic effects. The interdiffusion coefficient of Cr in β-Ti was successfully obtained,[49] but no value was reported concerning the diffusion behavior of Ti in Cr making the interpretation speculative. One possible explanation could be that the extension of the chemical gradient near the equilibrated interface is too small compared to the spatial resolution of the EPMA. Another interpretation could be that the Laves phase is formed rapidly at the interface in the early stages of the heat treatment. It could not only slow down the diffusion of atoms acting as a barrier, but the growth could also consume Cr atoms nearby, leading to depletion. Consequently, the solubility values of Ti in Cr obtained by diffusion couples were not considered. The analysis of the equilibrated alloys was also not conclusive at lower temperatures because the size of bcc precipitates was too small to be measured by EPMA. The tie-lines resulting from the application of Vegard's law were used as input to optimize the phase boundaries. Further studies were made in the ternary Cr–Mo–Ti system,[81] where the Laves phase stability and solubility of bcc were evaluated. Similar microstructures were obtained for Cr-rich samples, and the solubility was measured in a transmission electron microscope (TEM) by EDS. Applying this technique, spatial resolution was good enough to measure the chemical composition of each phase. The obtained solubility for alloys containing less than 1 at% Mo (i.e., very near to the binary Cr–Ti system) agrees with the applied Vegard's law (Fig. 4). In addition, the solubility of the bcc solution obtained by means of metallography reported in the literature was also considered.

Figure 9 shows the resulting calculated phase diagram of the present work compared with experimental data from this study and from the literature. A comparison with the assessments published by Cupid et al.[60] is shown in Fig. 10, and the respective calculated values of invariant reaction temperatures are listed in Table 6 together with the present experimental data. The assessed thermodynamic parameters could be obtained from "Supplementary information". The main improvement of the present phase diagram compared with previous works is the position of

the invariant reactions involving the *C*15 and *C*36 Laves phase. In this case, both reactions occur in a similar temperature range in contrast with previous assessments.

7 Conclusion

In the present work, the phase diagram and thermochemical properties of the Cr–Ti system were studied by a combined approach of experiments and calculations. The thermodynamic activity of the bcc solid solution was measured by KEMS. In contrast with previous studies,[36] the activity remains constant as a function of temperature. The stability of all three polymorphic structures of the Laves phases was determined by DTA. Measured temperatures for the transformation between the *C*36 and *C*14 Laves phases are in agreement with recent studies.[46] The difference of the temperature of transformation between the *C*15 and the *C*36 polytypes on both sides of the Laves phase is much smaller than reported previously. Equilibrated alloys and diffusion couples were used to measure the solubility of Cr and Ti in the bcc solid solution and to determine the equilibrium tie-lines with the corresponding Laves phase. Finally, DFT calculations were performed to set the enthalpy of formation of all end members of the Laves phases.

A thermodynamic reassessment of the system was carried out by a critical evaluation of available data and the present results. "As-calculated" DFT data was used to limit the number of optimized variables. A simplified sublattice model was successfully applied to describe the Laves phases using the coordination number as a criterion to merge different crystallographic sites. By reducing the number of sublattices, the quantity of parameters is considerably reduced when the description is applied to higher-order systems. The stability of the Laves phases of the proposed Cr–Ti phase diagram is much more like its analog Cr–Zr system. The new assessment of the Cr–Ti binary system can help in the understanding of Laves phase stability in ternary systems.

Supplementary Information The online version contains supplementary material available at https://doi.org/10.1007/s11669-024-01090-2.

Acknowledgment The authors thank Shigehiro Ishikawa for his contribution to the EPMA, DTA, and XRD experiments and Thierry Alpettaz for KEMS activity measurements.

References

1. H. Brearley, Cutlery, US1197256A, 1916.
2. B. Sun, X. Zuo, X. Cheng, and X. Li, The Role of Chromium Content in the Long-Term Atmospheric Corrosion Process, *Npj Mater. Degrad.*, 2020, **4**(1), p 1-9. https://doi.org/10.1038/s41529-020-00142-5
3. M.F. Ashby, Material and process selection charts, in: Mater. Sel. Mech. Des., 2nd ed, Butterworth-Heinemann, Boston, MA, 1999, p 413-466.
4. V.N. Svechnikov, M.Y. Teslyuk, Y.A. Kocherzhinsky, V.V. Petkov, and E.V. Dabizha, Three Modifications of $TiCr_2$, *Dopov. Akad. Nauk Ukr. RSR*, 1970, **32**(9), p 837-837. **in Ukranian**
5. J.D. Livingston, Laves-phase superalloys?, *Phys. Status Solidi Appl. Mater. Sci*, 1992, **131**(2), p 415-423. https://doi.org/10.1002/pssa.2211310215
6. M. Bououdina, D. Grant, and G. Walker, Review on Hydrogen Absorbing Materials-Structure, Microstructure, and Thermodynamic Properties, *Int. J. Hydrog. Energy*, 2006, **31**(2), p 177-182. https://doi.org/10.1016/j.ijhydene.2005.04.049
7. E. Akiba and H. Iba, Hydrogen Absorption by Laves Phase Related BCC Solid Solution, *Intermetallics*, 1998, **6**(6), p 461-470. https://doi.org/10.1016/S0966-9795(97)00088-5
8. F. Stein and A. Leineweber, Laves Phases: A Review of Their Functional and Structural Applications and an Improved Fundamental Understanding of Stability and Properties, *J. Mater. Sci.*, 2021, **56**(9), p 5321-5427. https://doi.org/10.1007/s10853-020-05509-2
9. J.N. Mundy, C.W. Tse, and W.D. McFall, Isotope Effect in Chromium Self-Diffusion, *Phys. Rev. B*, 1976, **13**(6), p 2349-2357. https://doi.org/10.1103/PhysRevB.13.2349
10. J.N. Mundy, H.A. Hoff, J. Pelleg, S.J. Rothman, L.J. Nowicki, and F.A. Schmidt, Self-Diffusion in Chromium, *Phys. Rev. B*, 1981, **24**(2), p 658-665. https://doi.org/10.1103/PhysRevB.24.658
11. U. Köhler and C. Herzig, On the Anomalous Self-Diffusion in B.C.C., Titanium, *Phys. Status Solidi B*, 1987, **144**(1), p 243-251. https://doi.org/10.1002/pssb.2221440122
12. N.E. Walsöe de Reca and C.M. Libanati, Autodifusion de Titanio Beta y Hafnio Beta, *Acta Metall.*, 1968, **16**(10), p 1297-1305. https://doi.org/10.1016/0001-6160(68)90010-2
13. T.B. Massalski, H. Okamoto, P.R. Subramanian, L. Kacprzak, Eds., *Binary Alloy Phase Diagrams* ASM International, Metals Park, 1990
14. F.C. Frank and J.S. Kasper, Complex Alloy Structures regarded As Sphere Packings. II. Analysis and Classification of Representative Structures, *Acta Crystallogr.*, 1959, **12**(7), p 483-499. https://doi.org/10.1107/S0365110X59001499
15. W. Baumann and A. Leineweber, Solid Solubility by Anti-Site Atoms in the C36-$TiCr_2$ Laves Phase Revealed by Single-Crystal x-ray Diffractometry, *J. Alloys Compd.*, 2010, **505**(2), p 492-496. https://doi.org/10.1016/j.jallcom.2010.06.117
16. K. Ioroi, Y. Aono, X. Xu, T. Omori, and R. Kainuma, Melting Point of Pure Cr and Phase Equilibria in the Cr-Si Binary System, *J. Phase Equilib. Diffus.*, 2022, **43**(2), p 229-242. https://doi.org/10.1007/s11669-022-00954-9
17. W. Zhuang, J. Shen, Y. Liu, L. Ling, S. Shang, Y. Du, and J.C. Schuster, Thermodynamic Optimization of the Cr-Ti System, *Z. Metallkd.*, 2000, **91**(2), p 121-127.
18. R. Vogel and B. Wenderott, Das Zustandsschaubild Eisen-Eisentitanid-Chromtitanid-Chrom, *Arch. für Eisenhüttenwes*, 1940, **14**(6), p 279-282. https://doi.org/10.1002/srin.194000912. **in German**
19. M.K. McQuillan, A Provisional Constitutional Diagram of the Chromium-Titanium System, *J. Inst. Met.*, 1951, **79**(11), p 379-390.
20. P. Duwez and J. Taylor, A Partial Titanium-Chromium Phase Diagram and the Crystal Structure of $TiCr_2$, *Trans. Am. Soc. Met.*, 1952, **44**, p 495-517.
21. R. van Thyne, H. Kessler and M. Hansen, The Systems Titanium-Chromium and Titanium-Iron, *Trans. Am. Soc. Met.*, 1952, **44**, p 974-989.

22. F. Cuff, N. Grant, and C. Floe, Titanium-Chromium Phase Diagram, *Trans. Am. Inst. Min. Metall. Eng.*, 1952, **194**(8), p 848-853.
23. B. Levinger, High Temperature Modification of $TiCr_2$, *Trans. Am. Inst. Min. Metall. Eng.*, 1953, **197**(2), p 196-196.
24. M.K. McQuillan, A Redetermination and Interpretation of the Titanium-Rich Region of the Titanium Chromium System, *J. Inst. Met.*, 1954, **82**(9), p 433-439.
25. I.I. Kornilov, V.S. Mikheev, and T.S. Chernova, Constitution Diagram of Ti-Cr, *Trudy Inst. Metall. Akad. Nauk SSSR*, 1957, **2**, p 126-134. **in Russian**
26. Y.A. Bagariatskii, G.I. Nosova, and T.V. Tagunova, Study of the Phase Diagrams of the Alloys Titanium-Chromium, Titanium-Tungsten, and Titanium-Chromium-Tungsten, Prepared by the Method of Powder Metallurgy, *Zh. Neorg. Khim.*, 1958, **3**(3), p 777-785. **in Russian**
27. A.W. Goldenstein, A.G. Metcalfe, and W. Rostoker, The Effect of Stress on the Eutectoid Decomposition of Titanium Chromium Alloys, *Trans. Am. Soc. Met.*, 1959, **51**, p 1036-1053.
28. K. Gross and I. Lamborn, Allotropic Modifications of $TiCr_2$, *J. Inst. Met.*, 1960, **88**(9), p 416-416.
29. I. Ageev, O. Karpinski, and L. Petrova, Stability of Beta-Solid Solution of Titanium-Chromium Alloys, *Zh. Neorg. Khim.*, 1961, **6**(8), p 1976-1978.
30. F. Ermanis, P. Farrar, and H. Margolin, A Reinvestigation of the Systems Ti-Cr and Ti-V, *Trans. Metall. Soc. Aime.*, 1961, **221**(5), p 904-908.
31. V.S. Mikheev and V.S. Aleksashin, Electrical Volume Resistivity of Alloys of the Titanium-Chromium System up to Temperatures of 1100 °C, *Fiz. Met. Metalloved.*, 1962, **14**(2), p 231-237.
32. V.S. Mikheyev and T.S. Chernova, Solubility of Chromium in α-Titanium and Mechanical Properties of the Binary System Titanium-Chromium, *Titan Ego Splavy SSSR Inst Met.*, 1962, **7**, p 35-73.
33. V.N. Svechnikov, Y.A. Kocherzhinskii, and V.I. Latysheva, Consitution Diagram of Chromium Titanium, *Vopr. Fiz. Met. Metalloved.*, 1962, **16**, p 132-135. **in Ukranian**
34. P. Farrar and H. Margolin, A Reinvestigation of Chromium-Rich Region of Titanium-Chromium System, *Trans. Metall. Soc. Aime.*, 1963, **227**(6), p 1342-1345.
35. N.V. Ageev and M.S. Model, Decay of Solid Solutions of Niobium and and Titanium in Chromium, *Dokl. Akad. Nauk SSSR*, 1963, **148**(1), p 84-85. **in Russian**
36. M. Pool, R. Speiser, and G. Pierre, Activities of Chromium and Titanium in Binary Chromium-Titanium Alloys, *Trans. Metall. Soc. Aime.*, 1967, **239**(8), p 1180-1186.
37. E. Rudy, Ternary Phase Equilibria in Transition Metal-Boron–Carbon–Silicon Systems. Part 5. Compendium of Phase Diagram Data, AFML-TR-65-2, Air Force Materials Laboratory, Air Force Systems Command, Wright-Patterson Air Force Base, OH, 1969.
38. S.A. Minayeva and P.B. Budberg, Phase Structure of Ti-Cr Alloys, *Russ. Metall.*, 1971, **4**, p 144-147.
39. F. Faudot, J. Bigot, Study of Chromium solubility in α pure-Titanium, Titanium Science and Technology, Proceedings of the Fifth International Conference on Titanium, Munich, Deutsche Gesellschaft für Metalkunde e. V., 1984, 3, p 1445-1449.
40. H. Kudielka, Zum Aufbau des Dreistoff-Systems Titan-Niob-Chrom, DFG Final Report, 1990.
41. M. Sluiter and P.E.A. Turchi, Phase Stability in Ti-V and Ti-Cr Alloys: A Theoretical Investigation, *Phys. Rev. B*, 1991, **43**(15), p 12251-12266. https://doi.org/10.1103/PhysRevB.43.12251
42. K.C. Chen, S.M. Allen, and J.D. Livingston, Stoichiometry and Alloying Effects on the Phase Stability and Mechanical Properties of $TiCr_2$-Base LAVES Phase Alloys, *MRS Online Proc. Libr.*, 1994, **364**, p 1401-1406. https://doi.org/10.1557/PROC-364-1401
43. K.C. Chen, S.M. Allen, and J.D. Livingston, Microstructures of two-Phase Ti–Cr Alloys Containing the $TiCr_2$ Laves Phase Intermetallic, *J. Mater. Res.*, 1997, **12**(6), p 1472-1480. https://doi.org/10.1557/JMR.1997.0203
44. K.C. Chen, S.M. Allen, and J.D. Livingston, Factors Affecting the Room-Temperature Mechanical Properties of $TiCr_2$-Base Laves Phase Alloys, *Mater. Sci. Eng. A*, 1998, **242**(1), p 162-173. https://doi.org/10.1016/S0921-5093(97)00526-1
45. J.C. Zhao, M.R. Jackson, and L.A. Peluso, Mapping of the Nb-Cr-Ti Phase Diagram Using Difusion Multiples, *Z. Metallkd.*, 2004, **95**(3), p 142-146. https://doi.org/10.3139/146.017927
46. W. Baumann, A. Leineweber, and E.J. Mittemeijer, The Kinetics of a Polytypic Laves Phase Transformation in $TiCr_2$, *Intermetallics*, 2011, **19**(4), p 526-535. https://doi.org/10.1016/j.intermet.2010.11.027
47. M. Chandran, P.R. Subramanian, and M.F. Gigliotti, First Principles Calculation of mIxing Enthalpy of β-Ti with Transition Elements, *J. Alloys Compd.*, 2013, **550**, p 501-508. https://doi.org/10.1016/j.jallcom.2012.10.141
48. R. Sahara, S. Emura, and K. Tsuchiya, Theoretical Investigation of Effect of Alloying Elements on Phase Stability in Body-Centered Cubic Ti-X alloys (X=V, Cr, Fe Co, Nb, and Mo), *J. Alloys Compd.*, 2015, **634**, p 193-199. https://doi.org/10.1016/j.jallcom.2015.02.005
49. L. Zhu, Q. Zhang, Z. Chen, C. Wei, G.-M. Cai, L. Jiang, Z. Jin, and J.-C. Zhao, Measurement of Interdiffusion and Impurity Diffusion Coefficients in the bcc Phase of the Ti–X (X = Cr, Hf, Mo, Nb, V, Zr) Binary Systems Using Diffusion Multiples, *J. Mater. Sci.*, 2017, **52**(6), p 3255-3268. https://doi.org/10.1007/s10853-016-0614-0
50. S. Xu, H. Zhang, G. Yang, Y. Liang, X. Xu, J. He, and J. Lin, Phase Equilibria in the Ti–Al–Cr System at 1000 °C, *J. Alloys Compd.*, 2020, **826**, 154236. https://doi.org/10.1016/j.jallcom.2020.154236
51. K. Ohsaka, E.H. Trinh, J.C. Holzer, and W.L. Johnson, Gibbs Free Energy Difference Between the Undercooled Liquid and the β PHase of a Ti-Cr Alloy, *Appl. Phys. Lett.*, 1992, **60**(9), p 1079-1081. https://doi.org/10.1063/1.106450
52. J.-C. Crivello, Private communication, SQS calculations of the BCC-Ti, 2022.
53. J. Pavlů, J. Vřešťál, and M. Šob, Thermodynamic Modeling of Laves Phases in the Cr–Hf and Cr–Ti Systems: Reassessment Using First-Principles Results, *Calphad*, 2010, **34**(2), p 215-221. https://doi.org/10.1016/j.calphad.2010.03.003
54. M.H.F. Sluiter, Lattice Stability Prediction of Elemental Tetrahedrally Close-packed Structures, *Acta Mater.*, 2007, **55**(11), p 3707-3718. https://doi.org/10.1016/j.actamat.2007.02.016
55. X.-Q. Chen, W. Wolf, R. Podloucky, and P. Rogl, Ab Initio Study of Ground-State Properties of the Laves Phase Compounds $TiCr_2$, $ZrCr_2$, and $HfCr_2$, *Phys. Rev. B*, 2005, **71**, 174101. https://doi.org/10.1103/PhysRevB.71.174101
56. L. Kaufman and H. Nesor, Coupled Phase Diagrams and Thermochemical data for Transition Metal Binary Systems - I, *Calphad*, 1978, **2**(1), p 55-80. https://doi.org/10.1016/0364-5916(78)90005-6
57. I. Ansara, A.T. Dinsdale, and M.H. Rand, COST 507: Thermochemical Database for Light Metal Alloys, Office for Official Publications of the European, *Communities*, 1998, **2**, p 1-420.
58. J.Y. Lee, J.H. Kim, S.I. Park, and H.M. Lee, Phase Equilibrium of the Ti–Cr–V Ternary System in the Non-Burning β-Ti alloy Region, *J. Alloys Compd.*, 1999, **291**(1), p 229-238. https://doi.org/10.1016/S0925-8388(99)00144-9

59. G. Ghosh, Thermodynamic and Kinetic Modeling of the Cr-Ti-V System, *J. Phase Equilibria.*, 2002, **23**(4), p 310-328. https://doi.org/10.1361/105497102770331569
60. D.M. Cupid, M.J. Kriegel, O. Fabrichnaya, F. Ebrahimi, and H.J. Seifert, Thermodynamic Assessment of the Cr–Ti and first Assessment of the Al–Cr–Ti Systems, *Intermetallics*, 2011, **19**(8), p 1222-1235. https://doi.org/10.1016/j.intermet.2011.03.031
61. H. Sun, Y. Zhang, Q. Pan, Y. Liu, W. Zheng, and X.-G. Lu, Thermodynamic Modeling of the Ni-Ti-Cr System and the B2/B19′ Martensitic Transformation, *Calphad*, 2022, **79**, 102505. https://doi.org/10.1016/j.calphad.2022.102505
62. H.M. Rietveld, A Profile Refinement Method for Nuclear and Magnetic Structures, *J. Appl. Crystallogr.*, 1969, **2**(2), p 65-71. https://doi.org/10.1107/S0021889869006558
63. A. Berche, C. Rado, O. Rapaud, C. Guéneau, and J. Rogez, Thermodynamic Study of the U-Si System, *J. Nucl. Mater.*, 2009, **389**(1), p 101-107. https://doi.org/10.1016/j.jnucmat.2009.01.014
64. P. Gardie, G. Bordier, J.J. Poupeau, and J. Le Ny, Thermodynamic Activity Measurements of U-Fe and U-Ga alloys by Mass Spectrometry, *J. Nucl. Mater.*, 1992, **189**(1), p 85-96. https://doi.org/10.1016/0022-3115(92)90422-H
65. M. Baıchi, C. Chatillon, C. Guèneau, and S. Chatain, Mass Spectrometric Study of UO_2–ZrO_2 Pseudo-Binary System, *J. Nucl. Mater.*, 2001, **294**(1), p 84-87. https://doi.org/10.1016/S0022-3115(01)00477-9
66. S. Chatain, T. Alpettaz, S. Gossé, and C. Guéneau, Thermodynamic Activity Measurements in Nickel-Base Industrial Alloys and Steels by Knudsen cell – Mass Spectrometry, *J. Chem. Thermodyn.*, 2017, **114**, p 144-150. https://doi.org/10.1016/j.jct.2017.01.015
67. J. Safarian and T.A. Engh, Vacuum Evaporation of Pure Metals, *Metall. Mater. Trans. A*, 2013, **44**(2), p 747-753. https://doi.org/10.1007/s11661-012-1464-2
68. Z.-K. Liu, Computational Thermodynamics and its Applications, *Acta Mater.*, 2020, **200**, p 745-792. https://doi.org/10.1016/j.actamat.2020.08.008
69. G. Kresse and J. Furthmüller, Efficiency of Ab-Initio Total Energy Calculations for Metals and Semiconductors using a Plane-Wave Basis Set, *Comput. Mater. Sci.*, 1996, **6**(1), p 15-50. https://doi.org/10.1016/0927-0256(96)00008-0
70. G. Kresse and D. Joubert, From Ultrasoft Pseudopotentials to the Projector Augmented-Wave Method, *Phys. Rev. B*, 1999, **59**(3), p 1758-1775. https://doi.org/10.1103/PhysRevB.59.1758
71. P.E. Blöchl, Projector Augmented-Wave Method, *Phys. Rev. B*, 1994, **50**(24), p 17953-17979. https://doi.org/10.1103/PhysRevB.50.17953
72. J.P. Perdew, K. Burke, and M. Ernzerhof, Generalized Gradient Approximation Made Simple, *Phys. Rev. Lett.*, 1996, **77**(18), p 3865-3868. https://doi.org/10.1103/PhysRevLett.77.3865
73. J.-C. Crivello, R. Souques, A. Breidi, N. Bourgeois, and J.-M. Joubert, ZenGen, a tool to Generate Ordered Configurations for Systematic First-Principles Calculations: The Cr–Mo–Ni–Re System as a Case Study, *Calphad*, 2015, **51**, p 233-240. https://doi.org/10.1016/j.calphad.2015.09.005
74. H.J. Monkhorst and J.D. Pack, Special Points for Brillouin-Zone Integrations, *Phys. Rev. B*, 1976, **13**(12), p 5188-5192. https://doi.org/10.1103/PhysRevB.13.5188
75. A.T. Dinsdale, SGTE data for pure elements, Calphad, 1991, 15(4), p 317-425. https://doi.org/10.1016/0364-5916(91)90030-N. Version 5.0 (2009) https://www.sgte.net/en/free-pure-substance-database
76. Z.H. Yan, T. Klassen, C. Michaelsen, M. Oehring, and R. Bormann, Inverse Melting in the Ti-Cr System, *Phys. Rev. B*, 1993, **47**(14), p 8520-8527. https://doi.org/10.1103/PhysRevB.47.8520
77. W. Baumann, Private Communication, DTA Experiments on the Cr-Ti System, 2012.
78. J.P. Gros, I. Ansara, M. Allibert, Prediction of alpha/beta equilibria in Titanium-based alloys containing Al, Mo, Zr, Cr (Part I), in: Societé Française de Métallurgie, Cannes, 1988, p 1553.
79. A. van de Walle, Q. Hong, S. Kadkhodaei, and R. Sun, The Free Energy of Mechanically Unstable Phases, *Nat. Commun.*, 2015, **6**(1), p 7559. https://doi.org/10.1038/ncomms8559
80. S. Kadkhodaei, Q.-J. Hong, and A. van de Walle, Free Energy Calculation of Mechanically Unstable but Dynamically Stabilized bcc Titanium, *Phys. Rev. B*, 2017, **95**(6), 064101. https://doi.org/10.1103/PhysRevB.95.064101
81. A. Flores, To be published, Experimental investigation of the Cr-Mo-Ti system, 2023.